

This is the peer reviewed version of the following article:

Effects of substituents on transport properties of molecular materials for organic solar cells: A theoretical investigation / Alberga, D., Ciofini, I., Mangiatordi, G.F., Pedone, A., Lattanzi, G., Roncali, J., Adamo, C.. - In: CHEMISTRY OF MATERIALS. - ISSN 0897-4756. - 29:2(2017), pp. 273-281. [10.1021/acs.chemmater.6b04277]

Terms of use:

The terms and conditions for the reuse of this version of the manuscript are specified in the publishing policy. For all terms of use and more information see the publisher's website.

11/06/2026 12:52

(Article begins on next page)

Effects of Substituents on Transport Properties of Molecular Materials for Organic Solar Cells: a Theoretical Investigation.

Domenico Alberga, Ilaria Ciofini, Giuseppe Felice Mangiatordi,
Alfonso Pedone, Gianluca Lattanzi, Jean Roncali, and Carlo Adamo

Chem. Mater., **Just Accepted Manuscript** • DOI: 10.1021/acs.chemmater.6b04277 • Publication Date (Web): 05 Dec 2016

Downloaded from <http://pubs.acs.org> on December 6, 2016

Just Accepted

“Just Accepted” manuscripts have been peer-reviewed and accepted for publication. They are posted online prior to technical editing, formatting for publication and author proofing. The American Chemical Society provides “Just Accepted” as a free service to the research community to expedite the dissemination of scientific material as soon as possible after acceptance. “Just Accepted” manuscripts appear in full in PDF format accompanied by an HTML abstract. “Just Accepted” manuscripts have been fully peer reviewed, but should not be considered the official version of record. They are accessible to all readers and citable by the Digital Object Identifier (DOI®). “Just Accepted” is an optional service offered to authors. Therefore, the “Just Accepted” Web site may not include all articles that will be published in the journal. After a manuscript is technically edited and formatted, it will be removed from the “Just Accepted” Web site and published as an ASAP article. Note that technical editing may introduce minor changes to the manuscript text and/or graphics which could affect content, and all legal disclaimers and ethical guidelines that apply to the journal pertain. ACS cannot be held responsible for errors or consequences arising from the use of information contained in these “Just Accepted” manuscripts.



Effects of Substituents on Transport Properties of Molecular Materials for Organic Solar Cells: a Theoretical Investigation.

Domenico Alberga,[†] Ilaria Ciofini,[†] Giuseppe Felice Mangiatordi,[‡] Alfonso Pedone,[¶] Gianluca Lattanzi,[§] Jean Roncali,^{*,||} and Carlo Adamo^{*,†}

[†]*Institut de Recherche de Chimie Paris CNRS Chimie ParisTech, PSL Research University, 11 rue P. et M. Curie, F-75005 Paris 05, France*

[‡]*Dipartimento di Farmacia - Scienze del Farmaco, Università di Bari "Aldo Moro", Via Orabona, 4, I-70126 Bari, Italy*

[¶]*Department of Chemical and Geological Sciences, University of Modena and Reggio Emilia, Via Campi 103, 41125 Modena, Italy*

[§]*Dipartimento di Fisica, Università di Trento, Via Sommarive 14, 38123 Povo-Trento, Italy*

^{||}*Group Linear Conjugated Systems, CNRS UMR 6200, Moltech-Anjou, University of Angers, 2 Bd Lavoisier, 49045 Angers, France*

E-mail: jeanroncali@gmail.com; carlo.adamo@chimie-paristech.fr

Abstract

We present a theoretical investigation of the effects of substitution of the triphenylamine (TPA) block on the overall properties of materials based on small push-pull molecules designed as donor for organic photovoltaics (OPV). In particular, we exploit modern computational techniques such as Density Functional Theory (DFT), Time-Dependent-DFT (TD-DFT), Molecular Dynamics (MD), and the Marcus theory,

1
2
3
4 to analyze the charge and exciton transport properties in crystalline and amorphous
5
6 phases of four compounds in which one phenyl ring of the TPA block of 2-((5-(4-
7
8 (methyl(phenyl)amino)phenyl)thiophen-2-yl)methylene)malononitrile is replaced by a
9
10 methyl, a α -naphthyl, and a β -naphthyl. Our calculations unveil the molecular rationale
11
12 behind the different transport properties observed in the experiments. We show that,
13
14 although the effects of the substituents on the electronic and optical properties are
15
16 negligible, they impact on the molecular packing of the crystalline structure, thus ex-
17
18 plaining the different macroscopic transport properties (observed and calculated). In
19
20 particular, the substitution of a phenyl with a methyl favors face-to-face $\pi - \pi$ packing
21
22 in the crystal structure and allows a good π -orbital overlap and high hopping rates.
23
24 On the contrary, the introduction of an α -naphthyl group generates a steric hindrance
25
26 that negatively affects the transport properties. Moreover, the investigated substitu-
27
28 tions do not significantly influence the degree of local order in the amorphous bulks
29
30 displaying complete disorder and low hole mobilities. These results, in agreement with
31
32 the experimental findings, suggest that our computational approach is able to account
33
34 for the macroscopic effect of subtle transformations of a molecular structure on trans-
35
36 port properties and thus can be further employed to obtain valuable insights for the
37
38 molecular design of optimized active materials for OPV.

39 40 41 **Keywords**

42
43
44 organic solar cells, HTM, DFT, MD, Marcus Theory

45 46 47 48 **Introduction**

49
50
51 Organic photovoltaics (OPV) is attracting increasing interest as an alternative to inorganic
52
53 solar cells due to possible applications in low-cost, low environmental impact, light-weight
54
55 and large-area flexible devices.¹⁻⁴ An organic solar cell (OSC) basically consists of the het-
56
57 erojunction created by contacting an electron donor material (D) with an electron-acceptor
58
59
60

1
2
3
4 (A).⁵ The basic functioning of an OSC consists in four steps: the absorption of an incident
5
6 photon by the active material (D in general) generates a bound electron-hole pair (exciton)
7
8 which diffuses in the D phase and dissociates at the D/A interface. The resulting electrons
9
10 and holes migrate in the D and A layers to be finally collected at the electrodes.^{1,2}

11
12 The performance of an OSC depends on the efficiency of these four steps that is af-
13
14 fected, in turn, by the properties of the materials employed in its fabrication. Its optimal
15
16 performance requires an improvement of the characteristics of each constituents.⁶

17
18 OSCs can be roughly divided into two main categories. Bi-layer planar heterojunctions
19
20 (PHJ) essentially fabricated by vacuum-deposition techniques^{7,8} and bulk heterojunction
21
22 solar cells (BHJ) in which the heterojunction created at the interface of segregated phases
23
24 of donor and acceptor materials is distributed in the entire volume of a solution-processed
25
26 active film. Besides fabrication by solution processes at room temperature, BHJs present
27
28 the advantage of a large increase of the area of the D/A interface and thus to a better
29
30 efficiency.^{9,10} Whereas soluble conjugated polymers have represented the major class of donor
31
32 materials for solution-processed BHJs for more than twenty years,¹¹ molecular donors have
33
34 recently emerged on the forefront of research on the chemistry of OPV materials due to
35
36 the advantages of well-defined chemical structures in terms of reproducibility of synthesis
37
38 and purification and possible analyses of structure-properties relationships.¹²⁻¹⁶ Thanks to
39
40 a multidisciplinary research effort focused on both the optimization of cell fabrication and
41
42 the synthesis of new donor materials, conversion efficiencies comparable to those obtained
43
44 with the best polymer-based cells (> 10%) have been recently reported for BHJ cells based
45
46 on molecular donors of relatively complex chemical structure.¹⁷ Besides high conversion
47
48 efficiency, a future industrial development of OPV depends on the possibility to offer decisive
49
50 economic and environmental advantages over existing technologies. In this context, the
51
52 development of active materials combining simple, cost-effective, clean and scalable synthesis
53
54 represents a key issue for the chemistry of OPV materials.¹⁸

55
56 In this work we focus on the donor materials. In particular, an efficient donor material for
57
58
59
60

1
2
3
4
5
6
7
8
9
10
11
12
13
14
15
16
17
18
19
20
21
22
23
24
25
26
27
28
29
30
31
32
33
34
35
36
37
38
39
40
41
42
43
44
45
46
47
48
49
50
51
52
53
54
55
56
57
58
59
60

OPV must combine:¹⁹ (1) good light-harvesting properties namely an absorption spectrum covering a large part of the solar irradiation spectrum and a high molecular extinction coefficient; (2) high hole mobility and exciton diffusion coefficient in order to minimize the transport resistance in the bulk; (3) large delocalization of the highest occupied molecular orbital (HOMO) that facilitates hole transport; (4) low HOMO energy level that increases the open circuit voltage (V_{oc}) of the solar cell; and (5) a high exciton diffusion coefficient and low exciton binding energy facilitating the exciton dissociation at the donor-acceptor interface.

A typical strategy employed to propose novel and more performing molecules consists in optimizing a reference skeleton with substituent groups that would enhance its charge and exciton transport properties.^{20–22} The structural change of the molecular scaffold is aimed at optimizing the relevant photovoltaic parameters of solar cells adopting these donor materials.

Recently, small triarylaminines-based (TAA) donor molecules have shown interesting photovoltaic performances.^{14,16,23,24} The number of TAA-based molecules studied within this context is huge, thus showing the fervent experimental interest on this subject.^{25–27} Owing to a combination of electron-donor properties and high hole-mobility TAA represent a major class of key building blocks for the design of metal-free chromophores for dye-sensitized solar cells^{28,29} and donor materials for OPV.^{12–16,21,30–32} Much work has already been devoted to the analysis of structure-properties relationships in TAA-based molecular donors for OPV and in particular, recent results on push-pull systems have shown that replacement of a phenyl groups of the triphenylaminines (TPA) block by some aromatic or aliphatic substituents has negligible impact on the electronic properties of the molecule but can induce dramatic changes in the charge-transport properties of the resulting materials. In particular, replacing an outer phenyl group of compound 2-((5-(4-(methyl(phenyl)amino)phenyl)thiophen-2-yl)methylene)malononitrile (**1**)³³ by a methyl group (**1-Me**) or the α -naphthyl group of **2a** by a β -naphthyl (**2b**) (Figure 1) leads to a significant increase of hole-mobility and photovoltaic conversion efficiency.^{32,34}

1
2
3 In this context computational techniques represent a powerful tool that allows to under-
4 stand, at the atomistic scale, the physical phenomena that lie behind the transport properties
5 unveiling the structure-property relationship in this class of molecules.^{22,35,36}
6
7

8
9
10 Theoretical studies based on classical Molecular Dynamics (MD) and quantum chemical
11 calculations were recently employed to fully characterize the structural, electronic, optical,
12 and transport properties of organic semiconductors in solar cells.³⁵⁻⁴¹ Charge and exciton
13 transport in organic semiconductors is commonly described as a hopping process whose rate
14 can be derived from the Marcus theory.⁴² This technique can be successfully used to calculate
15 the charge mobility, or the exciton diffusion coefficient, employing a master equation or the
16 Kinetic Monte Carlo (KMC) approach.^{43,44} The quantities entering the Marcus rates can be
17 calculated using the most appropriate level of theory depending on the complexity of the
18 studied system. In this context, it has been showed that Marcus rates calculations based
19 on the use of a semi-empirical Hamiltonian (ZINDO) produce reliable results that can be
20 compared to the experimental values. This technique is thus suitable to study transport on
21 large scales or complex systems.^{45,46} Not surprisingly this approach was successfully applied
22 to the study of hole transport in molecular and polymeric systems using configurations
23 extracted from MD simulations in the amorphous phase.^{36,39,47-49}
24
25
26
27
28
29
30
31
32
33
34
35
36
37

38 Framed in this picture, our study is aimed at investigating the four recently proposed
39 TAA-molecules³²⁻³⁴ depicted in Figure 1. We apply a modern computational approach
40 involving classical and quantum calculations and exploiting the Marcus theory in order to
41 shed light on the structure-properties relationship that rules the charge and exciton transport
42 in these systems in both crystalline and amorphous phases.
43
44
45
46
47

48 The paper is structured as follows: after a description of the employed computational
49 protocol, the calculated transport properties of the four investigated materials are discussed
50 in terms of their electronic, optical and packing properties. The results are presented in
51 the perspective of providing valuable insights to drive the rational design of new and better
52 performing molecules.
53
54
55
56
57
58
59
60

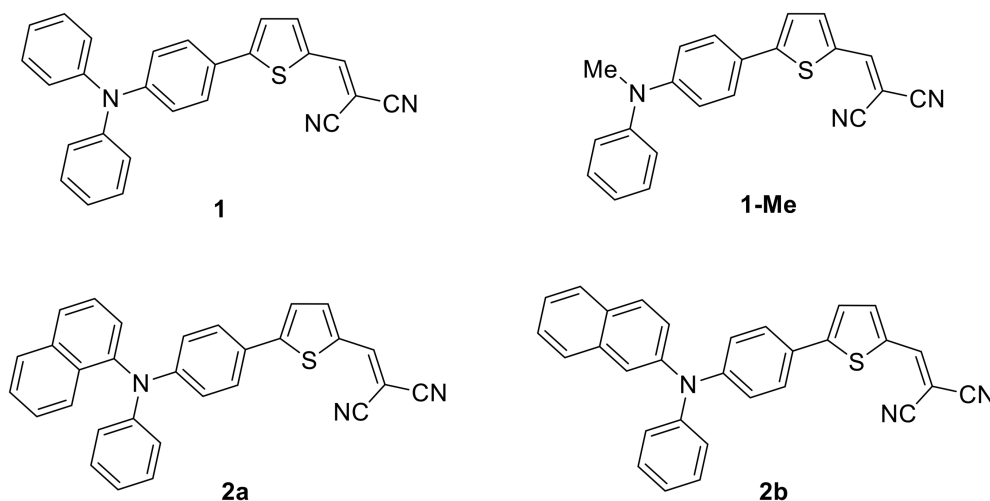


Figure 1: Chemical structures of the four TAA-based donor materials studied in this work.

Computational Methods

The crystal structures of the molecules **2a** and **2b** were obtained following the approach described in Ref. 35, by using the polymorph predictor module in Materials Studio.⁵⁰ A single molecule was optimized using the DMol3 module while electrostatic potential charges of all atoms were obtained employing the PBE functional.⁵¹ Crystal structure prediction was thus carried out using the Dreiding force field,⁵² considered the most reliable force field for molecular crystal prediction.⁵³ The polymorph predictor calculations were restricted to the five most probable space groups, i. e. P21/C, P1, P212121, P21, and $P\bar{1}$.⁵⁴ We sorted the obtained crystal structures as a function of their total energies and we selected those with the lowest energies.

MD simulations of the amorphous bulk⁵⁵ were performed for each compound to calculate the associated hole mobilities. Each system was built starting from a configuration in which 1000 molecules were placed at random positions in a cubic periodic box having an edge of 250 Å. All systems were equilibrated in the NPT ensemble at atmospheric pressure and high temperature ($P = 1$ atm, $T = 800$ K) until the volume of the periodic box reached an equilibrium value. Following a further equilibration run at $T = 300$ K, a 30-ns long trajectory in the NPT ensemble was obtained for each system. All MD simulations employed a

time step of 1 fs. A cutoff of 12 Å was applied to the van der Waals interactions through a switching function, whereas the particle mesh Ewald (PME) method was employed to calculate the electrostatic interactions. The simulations were performed using NAMD2.11 package⁵⁶ and the CGenFF force field.^{57,58} For all considered systems, the restrained electrostatic potential (RESP) procedure⁵⁹ was employed to obtain accurate partial charges (based on HF/6-31G(d,p) results). The equilibrium condition was ensured by verifying that the volume fluctuated around its average value: the plot of the volume of the simulation cell in the 30 ns-long NPT production run shows that the volume is at equilibrium in all the four cases (data in Figure S1 of Supporting Information).

To simulate the hole transport in each of the four systems in crystalline and amorphous phase, we applied the nonadiabatic high-temperature limit of the semiclassical Marcus charge-transfer theory.⁴² This theory is based on the assumption that charges are localized on a single molecule and charge-transfer reactions take place via a hopping mechanism according to which the hopping rate between two molecules i and j can be computed as

$$\omega_{ij} = \frac{J_{ij}^2}{\hbar} \sqrt{\frac{\pi}{\lambda k_B T}} \exp \left[-\frac{(\Delta E_{ij} - \lambda)^2}{4\lambda k_B T} \right] \quad (1)$$

where T is the temperature, J_{ij} is the electronic coupling element (or transfer integral) between i and j , $\Delta E_{ij} = E_i - E_j$ is the site energy difference, and λ is the reorganization energy.⁴²

The reorganization energy is defined as

$$\lambda = E_{nC} - E_{nN} + E_{cN} - E_{cC} \quad (2)$$

where E_{nN} (E_{cC}) is the electronic energy of the neutral (charged) molecule in its optimized neutral (charged) geometry and E_{nC} (E_{cN}) is the energy of the neutral (charged) molecule in the optimized charged (neutral) geometry. For the four molecules λ was calculated employing the density functional theory (DFT) at the B3LYP/6-311g(d,p) level of theory.

1
2
3
4
5
6
7
8
9
10
11
12
13
14
15
16
17
18
19
20
21
22
23
24
25
26
27
28
29
30
31
32
33
34
35
36
37
38
39
40
41
42
43
44
45
46
47
48
49
50
51
52
53
54
55
56
57
58
59
60

The electronic coupling elements were calculated following the approach presented in Ref. 46. The latter assumes that the HOMO orbital of a dimer results exclusively from the interaction of the HOMO orbitals ϕ_i and ϕ_j of the monomers i and j respectively and thus it can be expanded in terms of those. Within this approach $J_{ij} = \langle \phi_i | \hat{H} | \phi_j \rangle$, where \hat{H} is the dimer Hamiltonian. All J_{ij} s were calculated using the semi-empirical ZINDO method.^{45,60}

J_{ij} were calculated using the semi-empirical ZINDO method.^{45,60} It has been showed that the ZINDO Hamiltonian produce reliable results comparable to the experimental values. This technique is thus suitable to study transport in large scale or complex systems.^{45,46}

The site energy difference contains three contributions: 1) the internal site energy difference ($\epsilon_i - \epsilon_j$), 2) the electrostatic site energy difference calculated within a given volume around the pair using partial charges generated via the Merz-Singh-Kollman scheme⁶¹ and 3) the contributions of an applied external electric field \vec{E} ($\Delta E_{ext} = -e\vec{E} \cdot \vec{r}_{ij}$) where \vec{r}_{ij} is the vector joining the centers of mass of two molecules.

We calculated the Marcus rates for each molecular pair ij from a neighbor list built with a cutoff of 15 Å . In the case of molecular crystals, we neglected the internal and electrostatic contributions to the site energy difference due to the symmetry of the crystalline phase. For the calculation of the charge mobility in the amorphous phase we used molecular configurations extracted from MD simulations.

Finally, we calculated the hole mobilities μ setting up KMC simulations using the obtained rates. The mobility in the direction of the applied external electric field was calculated as

$$\mu = \frac{\langle v \rangle}{E} \quad (3)$$

where $\langle v \rangle$ is the average velocity of the charge in the direction of the applied field \vec{E} .

The exciton diffusion coefficients D for the four investigated systems in the crystalline phase were calculated following the approach described in Ref. 44. Likewise the charge transport, the exciton transport can be depicted as a hopping process with a hopping rate

described by Eq.1. In this case the reorganization energy λ is defined as⁶²⁻⁶⁴

$$\lambda = E_{nX} - E_{nN} + E_{xN} - E_{xX}, \quad (4)$$

where E_{nN} (E_{xX}) is the electronic energy of the molecule in the ground (excited) state of its optimized ground (excited) state geometry and E_{nX} (E_{xN}) is the energy of the molecule in the ground (excited) state of the optimized excited (ground) state geometry. For the four molecules λ was calculated with DFT calculations optimizing the ground and excited state geometries at the CAM-B3LYP/6-311G(d,p) level and calculating the four terms in Eq.4 at the B3LYP/6-311G(d,p) level of theory through single point calculations.

The excitonic couplings J_{ij} are defined as^{44,65,66}

$$J_{ij} = \frac{E_{Dim(2)} - E_{Dim(1)}}{2} \quad (5)$$

where $E_{Dim(1)}$ and $E_{Dim(2)}$ are the energies of the two lowest excited states of the dimer resulting from the Davydov splitting⁶⁷ of the monomer S_1 levels computed at the CAM-B3LYP/6-311G(d,p) level of theory.

The site energy difference contains only one term derived from the application of a small fictitious drift force \vec{F} ($\Delta E_{ij} = \vec{F} \vec{r}_{ij}$). This term was introduced in Ref. 44: the calculations of the exciton diffusion coefficient by means of a simple diffusion rate equation based on the hopping rates and the squared hopping distance possibly leads to an overestimation of the diffusion constant.⁶⁵ To overcome this issue, the authors suggest to apply a small fictitious force \vec{F} as a drift term in order to evaluate an exciton mobility in analogy with the charge mobility. The latter, combined with the Einstein relation, leads to

$$D = k_B T \frac{\langle v \rangle}{F} \quad (6)$$

where $\langle v \rangle$ is the average velocity of the exciton in the direction of \vec{F} . Similarly to the

1
2
3 calculation of hole mobility, D was calculated by means of KMC simulations using the
4
5 obtained rates.
6

7 In our charge and exciton transport models we neglected recombination phenomena as-
8
9 suming the same recombination rates for all the studied materials.
10

11 In the follow, DFT-based quantities calculated in implicit solvent are computed using
12
13 the polarizable continuum model (PCM). approach.⁶⁸
14
15

16 17 18 Results and Discussion 19

20
21 In order to calculate the hole mobility and the exciton diffusion coefficient in the investigated
22
23 systems in both crystalline and amorphous phase we first predicted the crystal structure
24
25 of the molecules **1**, **2a** and **2b** using Material Studio and the procedure described in the
26
27 Computational Methods section. All the obtained structures belong to the same space
28
29 group $P\bar{1}$ as the experimentally available crystal structure of the molecule **1-Me**.³² Table 1
30
31 reports the predicted cell parameters for the four crystals depicted in Figure 2.
32
33

34 Table 1: Cell parameters of the predicted crystalline structure of **2a** and **2b** along with the
35
36 experimental values of **1**³³ and **1-Me**.³² (Angles are reported in degrees and cell parameters
37
38 in Å).
39

System	α	β	γ	a	b	c
1 ^a	90.0000	90.0000	110.6000	19.8370	15.6120	7.1912
1-Me ^b	82.5470	84.1080	87.1230	5.7003	8.7382	17.5060
2a	67.6937	73.3101	76.4538	23.2413	8.1118	7.9374
2b	54.9466	82.2253	83.2363	19.1165	12.3813	7.1568

40
41
42
43
44
45 ^a experimental values are taken from Ref. 33

46 ^b experimental values are taken from Ref. 32
47
48

49 In conjugated molecules, the $\pi - \pi$ packing mode of the dimers inside the crystals plays
50
51 an important role in determining the hole mobility. In general, configurations characterized
52
53 by a cofacial $\pi - \pi$ packing allow an optimal π -orbital overlap that in turn ensures relatively
54
55 large transfer integrals.³⁵ A first qualitative inspection of the crystals shows that among all
56
57 molecules, **1-Me** and **2b** have the best geometrical packing that favors face-to-face $\pi - \pi$
58
59
60

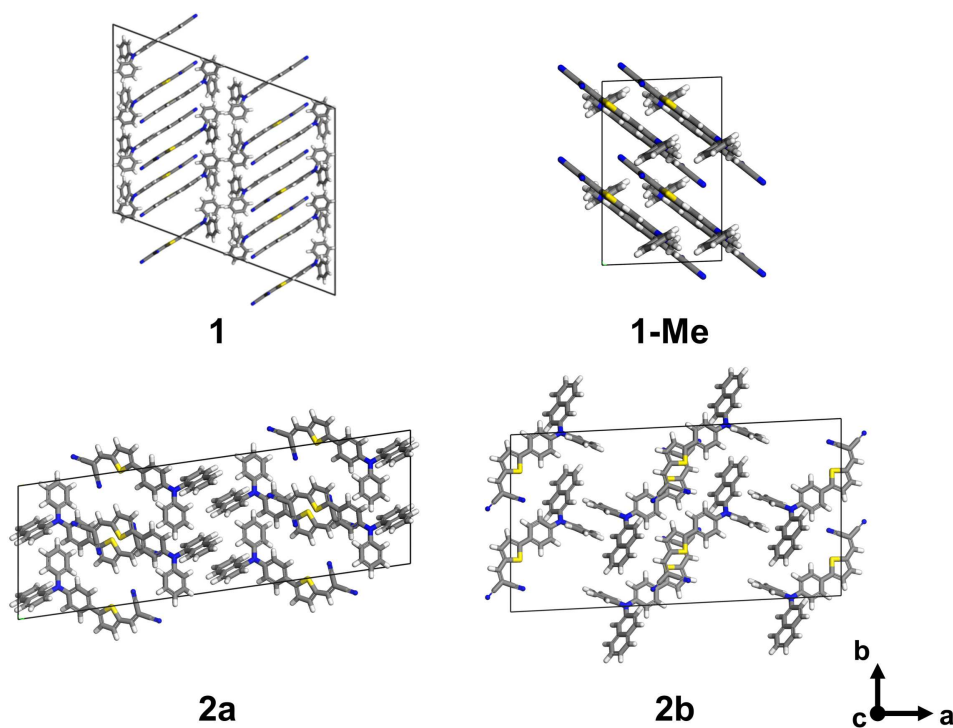


Figure 2: $2 \times 2 \times 2$ supercells of the predicted crystalline structures of **2a** and **2b** and of the experimental structures of **1-Me**³² and **1**.³³

stacking thus enhancing the transport properties.

Using the obtained crystal structures, we calculated the hole mobilities and the exciton diffusion coefficients of supercells ($3 \times 3 \times 5$ for **1**, $5 \times 5 \times 3$ for **1-Me** and $3 \times 5 \times 5$ for the others) along the three crystal axes (μ_a , μ_b , μ_c) as described in the Computational Methods section. For the calculation of the hole mobility we applied an electric field of 10^6 V/m. This value is typical in experimental measurements of charge mobility performed through the time-of-flight (TOF) technique.^{60,69} The results along with the average mobilities calculated in the three directions (μ_{av}) and the available experimental values (μ_{exp}) are reported in Table 2.

The calculated μ_{av} values show the same trend of the experimentally observed hole mobilities thus supporting the robustness of our calculation protocol.

For the calculation of the exciton diffusion coefficients of the four crystalline systems we employed a force of 16 aN in Eq. 1 as in Ref. 44. The calculated values in the direction of the three crystal axes (D_a , D_b , D_c) and the average values (D_{av}) are reported in Tab.3.

Table 2: Experimental μ_{exp} and calculated hole mobilities along the three crystallographic axes (μ_a , μ_b , μ_c) and their averages (μ_{av}) in $\text{cm}^2\text{V}^{-1}\text{s}^{-1}$. Computed reorganization energies (λ) are given in meV.

System	μ_a	μ_b	μ_c	μ_{av}	μ_{exp}^a	λ
1	$2.52 \cdot 10^{-5}$	$7.50 \cdot 10^{-5}$	$1.14 \cdot 10^{-4}$	$7.14 \cdot 10^{-5}$	$1.00 \cdot 10^{-5}$	127
1-Me	$6.03 \cdot 10^{-4}$	$2.45 \cdot 10^{-4}$	$4.77 \cdot 10^{-4}$	$4.42 \cdot 10^{-4}$	$5.00 \cdot 10^{-4}$	194
2a	$1.17 \cdot 10^{-5}$	$1.03 \cdot 10^{-5}$	$8.76 \cdot 10^{-6}$	$1.03 \cdot 10^{-5}$	$4.20 \cdot 10^{-6}$	156
2b	$1.68 \cdot 10^{-4}$	$1.14 \cdot 10^{-4}$	$1.09 \cdot 10^{-4}$	$1.30 \cdot 10^{-4}$	$5.50 \cdot 10^{-5}$	120

^a experimental values from Ref. 32,34

Table 3: Exciton diffusion coefficients calculated along the three crystallographic axes (D_a , D_b , D_c) and the average values D_{av} in m^2s^{-1} . Computed reorganization energies (λ) are given in meV.

System	D_a	D_b	D_c	D_{av}	λ
1	$2.18 \cdot 10^{-5}$	$2.94 \cdot 10^{-5}$	$4.17 \cdot 10^{-5}$	$3.10 \cdot 10^{-5}$	119
1-Me	$6.94 \cdot 10^{-5}$	$1.93 \cdot 10^{-5}$	$1.88 \cdot 10^{-5}$	$3.58 \cdot 10^{-5}$	128
2a	$4.26 \cdot 10^{-5}$	$2.86 \cdot 10^{-5}$	$1.96 \cdot 10^{-5}$	$3.03 \cdot 10^{-5}$	142
2b	$4.22 \cdot 10^{-6}$	$1.77 \cdot 10^{-5}$	$2.95 \cdot 10^{-5}$	$1.71 \cdot 10^{-5}$	138

The calculated D_{av} coefficients are similar for the four systems. In particular **1-Me** shows a slightly higher value in agreement with the highest power conversion efficiency (PCE) measured in solar cells making use of these molecules.^{32,34}

On the other hand, it is difficult to find a direct connection between the different transport properties calculated and the chemical structure of the analyzed molecules. First, the difference in both charge and excitonic reorganization energies reported in Table 2 and 3 respectively are too small to justify our results. Moreover, and to some extent unexpectedly, the molecule with the highest λ for hole transport, that is **1-Me**, displays also the highest hole mobility. The rationale that lies behind the different transport properties has thus to be found elsewhere.

At first, we looked for possible differences in the electronic and optical properties of the four molecules. Figure 3 shows the HOMO and LUMO orbitals computed for all systems.

It is clear that there is only a trifling difference in the frontier molecular orbitals among the molecules and that the influence of the substituents in the triphenylamine unit on the

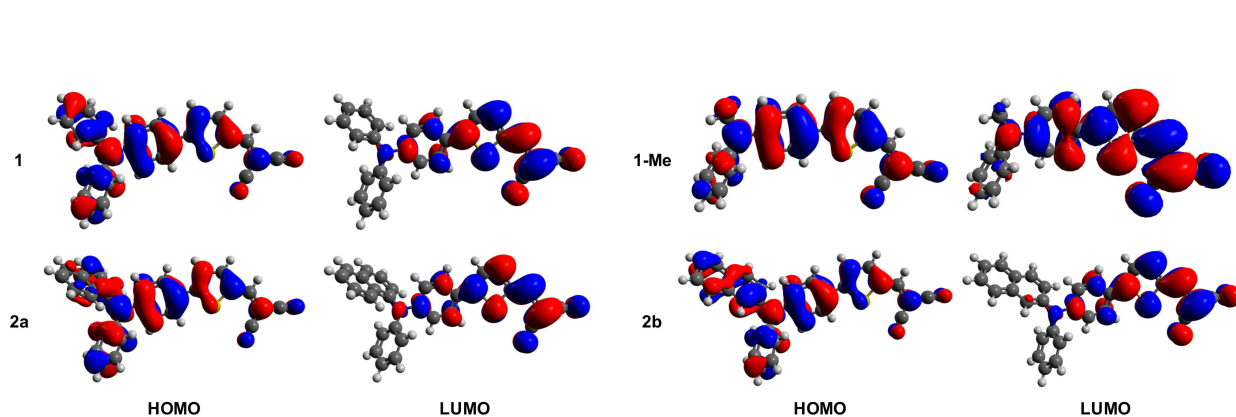


Figure 3: Computed HOMO and LUMO orbitals of the four investigated molecules calculated at B3LYP/6-311G(d,p) level of theory.

overall electronic structure is negligible. Moreover, we calculated (at the B3LYP/6-311G(d,p) level) other relevant parameters that depends on the electronic structure of the investigated molecules and that can influence the performance of a solar cell, namely: the HOMO-LUMO gap (Δ_{H-L}), the adiabatic ionization potential (IP) and the degree of charge delocalization (D_{chg}) defined as the ratio of the number of atoms of the molecule in the cationic state carrying a partial charge larger than 0.1e and the total number of atoms.³⁶

Table 4: Energies of the HOMO and LUMO orbitals (E_H and E_L) calculated at the B3LYP/6-311G(d,p) level along with the HOMO-LUMO gap Δ_{H-L} , the Adiabatic Ionization Potential (IP) expressed in eV and the degree of charge delocalization.

System	E_H	E_L	Δ_{H-L}	IP	D_{chg}
1	-5.57	-2.96	2.61	6.66	0.51
1-Me	-5.62	-2.84	2.77	6.77	0.52
2a	-5.58	-2.94	2.63	6.61	0.51
2b	-5.54	-2.97	2.57	6.57	0.52

The results are in qualitative agreement with the experimental values reported in Ref. 32,34. However, there are no appreciable differences among the studied systems except for **1-Me**: the substitution of an aromatic ring of the triphenylamine unit with a methyl group slightly increase both the Δ_{H-L} and the IP. Apart from that, the substituents in the triphenylamine unit have only a negligible effect on the electronic properties of the HTMs.

It might be argued that the systems could differ in their optical properties. To test this hypothesis, we computed the absorption (λ_{abs}) and emission wavelengths (λ_{em}) and

their difference (Stoke shift), at the TD-B3LYP/6-311G(d,p) level of theory. Their values are reported in Table 5, along with the optical gap, defined as the first singlet excitation energy E_1 ,⁷⁰ and the exciton binding energy E_b . The latter represents the energy required to fully separate the electron-hole pair against Coulomb attraction: it is defined as the energy difference between the neutral exciton and the two free charge carriers (i. e. the electron and the hole). This quantity is expressed as $E_b = E_g - E_1 = \Delta_{H-L} - E_1$. E_g is the electronic band gap, here replaced by the HOMO-LUMO energy gap (Δ_{H-L}).

Table 5: Optical properties calculated at the TD-B3LYP/6-311G(d,p) level of theory in implicit dichloromethane (Polarizable Continuum Model approach⁶⁸): the absorption λ_{abs} and the emission wavelengths λ_{em} based on S_0 and S_1 states along with the Stoke shifts in nm, the first singlet excitation energy E_1 and the exciton binding energy E_b in eV.

System	λ_{abs}	λ_{em}	Stoke shift	E_1	E_b
1	552	580	27	2.24	0.29
1-Me	515	540	25	2.40	0.25
2a	544	585	41	2.27	0.30
2b	559	590	31	2.21	0.29

1, **2a** and **2b** share analogous optical properties but in **1-Me** the substitution of an aromatic ring of the triphenylamine unit with a methyl leads to a blueshift for both emission and absorption. Moreover, there is a slight reduction of the exciton binding energy (E_b), which indicates that the electron-hole separation is favored in **1-Me**, thus increasing the performance of the solar cell.

Again, these small changes observed for the electronic and optical features of the four molecules cannot justify overall their difference in transport properties. These latter can thus be ascribed only to the different molecular packing in their crystalline phases induced by the small modifications in their molecular skeleton. Table 6 reports the centroid to centroid distance (r_{ij}), the square of the electronic coupling elements ($J_{ij}^{2(hole)}$ and $J_{ij}^{2(ex)}$) and the hopping rates ($\omega_{ij}^{(hole)}$ and $\omega_{ij}^{(ex)}$) computed for the main hopping pathways for hole and exciton transport in the four systems showed in Figure 4.

It is clear that among the investigated molecules **2b** and, especially, **1-Me** achieve the

Table 6: Centroid to centroid distance r_{ij} (\AA), the square of the electronic coupling elements ($J_{ij}^{2(hole)}$ and $J_{ij}^{2(ex)}$ in meV^2) and the hopping rates ($\omega_{ij}^{(hole)}$ and $\omega_{ij}^{(ex)}$ in s^{-1}) of the main hopping pathway of hole and exciton transport in the investigated systems.

System	r_{ij}	$J_{ij}^{2(hole)}$	$\omega_{ij}^{(hole)}$	$J_{ij}^{2(ex)}$	$\omega_{ij}^{(ex)}$
1	8.39	1.97	$1.74 \cdot 10^{13}$	95.5	$1.98 \cdot 10^{14}$
1-Me	5.70	7.37	$4.31 \cdot 10^{13}$	146.3	$2.92 \cdot 10^{14}$
2a	13.43	0.11	$1.03 \cdot 10^{12}$	117.5	$1.56 \cdot 10^{14}$
2b	10.86	2.28	$3.62 \cdot 10^{13}$	66.1	$5.19 \cdot 10^{13}$

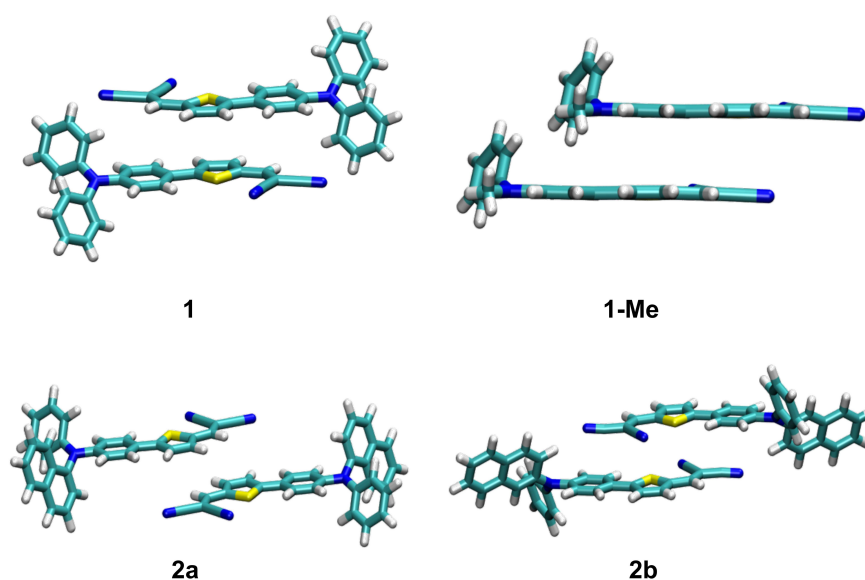


Figure 4: Main hopping pathway of hole transport in the investigated systems.

best packing in the molecular crystal. In particular, the substitution of the phenyl with a methyl in **1-Me** enhances the face to face $\pi - \pi$ packing and allows a good π -orbital overlap and a short centroid to centroid distance thus enhancing the transfer integrals and the hopping rates (see Table 6 and Figure 4). On the contrary, in **1** and **2a** the crystal packing forces the conjugated rings to a more tilted configuration and increase the distance between the centroids, thus negatively affecting the orbital overlap and the transport properties. Notably, there is a sensible difference in the calculated hole mobility between **2a** and **2b**. These two compounds both present a naphthyl group but a different connectivity. The β -

1
2
3
4
5
6
7
8
9
10
11
12
13
14
15
16
17
18
19
20
21
22
23
24
25
26
27
28
29
30
31
32
33
34
35
36
37
38
39
40
41
42
43
44
45
46
47
48
49
50
51
52
53
54
55
56
57
58
59
60

naphtyl compound (**2b**) shows a more coplanar geometry with respect to the α -naphtyl one (**2a**) that leads to a higher hole mobility. This is related to the larger steric hindrance of the α -naphtyl group that generates a more twisted structure, negatively affecting the transport properties.

In the case of the four HTMs in the amorphous phase, for each system we calculated the hole mobility for 1000 configurations extracted from the MD simulations as described in the Computational Methods section. The calculations were repeated applying an electric field of 10^6 V/m in several directions and averaging the resulting mobility values (μ_{amo}). The results are reported in Table7

Table 7: Hole mobilities calculated in the amorphous systems (μ_{amo} , in $\text{cm}^2\text{V}^{-1}\text{s}^{-1}$).

System	μ_{amo}
1	$(8.14 \pm 3.93) \cdot 10^{-11}$
1-Me	$(3.13 \pm 1.31) \cdot 10^{-11}$
2a	$(2.21 \pm 1.47) \cdot 10^{-11}$
2b	$(1.73 \pm 0.69) \cdot 10^{-10}$

The analyzed systems show similar low mobilities indicating a similar degree of local order in the amorphous phase. This is clearly evident from the calculation of the radial distribution function of the nitrogen atom belonging to the triphenylamine groups reported in Figure 5.

The radial distribution function is defined as the ratio^{55,71}

$$g(r) = N(r)/g_I(r) \quad (7)$$

where $N(r)$ is the number of occurrences of the radial distance r between pairs of particles and $g_I(r)$ is the radial distribution function of an ideal gas with density ρ : $g_I(r) = 4\pi\rho r^2$. Using this type of normalization $g(r \rightarrow \infty) = 1$. The presence of peaks in the $g(r)$ would reveal the presence of ordered structures in the bulk.

Figure 5 shows a similar $g(r)$ for all the investigated systems: the differences in terms of molecular structure among the four molecules are too small to significantly influence the

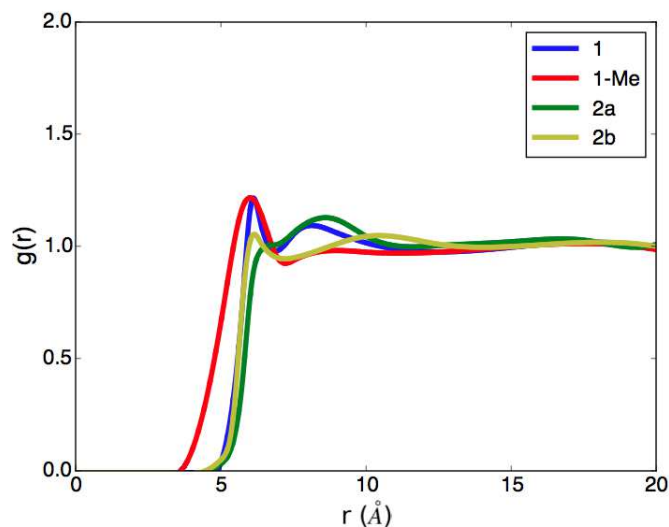


Figure 5: Radial distribution functions $g(r)$ of the nitrogen atom belonging to the triphenylamine groups of the simulated systems calculated from the MD trajectories in the amorphous phase.

local order properties of the amorphous bulks. Their similar low mobility values suggest that the amorphous domains of a typically polycrystalline HTM layer of a solar cell affect in analogous fashion the overall performance of the device.

Taken together, these results suggest that small modifications in the molecular structure of triphenylamine based HTMs are able to strongly affect their transport properties in the crystalline phase. Importantly, our calculations show that the substitution of a phenyl in the triphenylamine unit does not significantly alter the electronic and optical properties of these materials. On the other hand the tiny alteration of the molecular scaffold has a large effect on the molecular packing in the crystal structure. In particular, we show that the substitution of the phenyl with a methyl in **1-Me** enhances the face-to-face $\pi - \pi$ packing in the crystal structure increasing the effective π -orbital overlap and thus raising the hole mobility between conjugated molecules (see Table 6 and Figure 4). Moreover, we show that the molecular modifications do not alter significantly the low hole mobility of these materials in bulk amorphous phase that is completely disordered for all systems.

The theoretical results, in agreement with the experimental findings^{32,34} indicate that in

1
2
3 order to improve the transport properties and, consequently, the performance of a solar cell
4 it is important to focus on the crystal phase of the HTM materials designing molecules that
5 are able to achieve the most suitable molecular packing for transport.
6
7
8
9

10 11 12 Conclusions

13
14
15 In this study, we theoretically investigate the effects of small molecular substitutions in
16 the structure of triphenylamine based hole transporter materials used in organic solar cells
17 on their transport properties in the crystalline and amorphous phases. Exploiting DFT,
18 TD-DFT, MD, and the Marcus theory we analyze the molecular rationale that lies behind
19 the different measured transport properties of four HTMs whose scaffold differs only for
20 the substitution of one phenyl ring in the triphenylamine unit. Our calculations clearly
21 show that the effect of the substituents on the electronic and optical properties of these
22 materials is negligible. On the other hand, chemical modifications have important effects on
23 the molecular packing in the crystalline structure that are able to account for the different
24 calculated transport properties. In particular, we show that the substitution of the phenyl
25 with a methyl in **1-Me** enhances the face-to-face $\pi - \pi$ packing in the crystal structure
26 that allows a good π -orbital overlap at short centroid to centroid distance enhancing the
27 transfer integrals and the hopping rates. On the contrary, the presence of a α -naphthyl in **2a**
28 generates a twisted structure due to the steric hindrance that negatively affects its transport
29 properties.
30
31
32
33
34
35
36
37
38
39
40
41
42
43
44
45

46 Moreover we find that the difference in the molecular structure of the four molecules is
47 too small to significantly influence the degree of local order in the amorphous bulks all char-
48 acterized by a completely disordered morphology and low mobilities. In fact, the amorphous
49 phase is more sensitive to the overall shape of the molecules rather than to the effective
50 chemical substitutions. In the case of the materials studied in this work, the modification of
51 the molecular shape is too slight to affect the amorphous phase.
52
53
54
55
56
57
58
59
60

1
2
3
4
5
6
7
8
9
10
11
12
13
14
15
16
17
18
19
20
21
22
23
24
25
26
27
28
29
30
31
32
33
34
35
36
37
38
39
40
41
42
43
44
45
46
47
48
49
50
51
52
53
54
55
56
57
58
59
60

These results, in line with the experimental findings, suggest that in the quest of new performing materials able to improve the performances of a solar cell it is desirable to devise a strategy that, starting from little transformations of a molecular scaffold, leads to the optimization of the packing properties in the crystal phase and, consequently, to improved transport properties and more efficient solar cells.

Acknowledgement

We acknowledge the CINECA awards HP10CAJ6KE and HP10BWMW76 under the ISCRA initiative for the availability of high performance computing resources and support.

Supporting Information Available

Volume convergence plot. This material is available free of charge via the Internet at <http://pubs.acs.org/>.

References

- (1) Brabec, C.; Scherf, U.; Dyakonov, V. *Organic Photovoltaics: Materials, Device Physics, and Manufacturing Technologies*, John Wiley & Sons, 2011.
- (2) Günes, S.; Neugebauer, H.; Sariciftci, N. S. Conjugated Polymer-Based Organic Solar Cells. *Chem. Rev.* **2007**, *107*, 1324–1338.
- (3) Cao, W.; Xue, J. Recent Progress in Organic Photovoltaics: Device Architecture and Optical Design. *Energy Environ. Sci.* **2014**, *7*, 2123–2144.
- (4) Mazziio, K. A.; Luscombe, C. K. The Future of Organic Photovoltaics. *Chem. Soc. Rev.* **2015**, *44*, 78–90.

- 1
2
3
4
5
6
7
8
9
10
11
12
13
14
15
16
17
18
19
20
21
22
23
24
25
26
27
28
29
30
31
32
33
34
35
36
37
38
39
40
41
42
43
44
45
46
47
48
49
50
51
52
53
54
55
56
57
58
59
60
- (5) Tang, C. W. Two-layer Organic Photovoltaic Cell. *Appl. Phys. Lett.* **1986**, *48*, 183–185.
- (6) Kaur, N.; Singh, M.; Pathak, D.; Wagner, T.; Nunzi, J. Organic Materials for Photovoltaic Applications: Review and Mechanism. *Synth. Met.* **2014**, *190*, 20–26.
- (7) Wöhrle, D.; Meissner, D. Organic Solar Cells. *Adv. Mater.* **1991**, *3*, 129–138.
- (8) Peumans, P.; Yakimov, A.; Forrest, S. R. Small Molecular Weight Organic Thin-Film Photodetectors and Solar Cells. *J. Appl. Phys.* **2003**, *93*, 3693–3723.
- (9) Yu, G.; Gao, J.; Hummelen, J. C.; Wudl, F.; Heeger, A. J. Polymer Photovoltaic Cells: Enhanced Efficiencies via a Network of Internal Donor-Acceptor Heterojunctions. *Science* **1995**, *270*, 1789–1791.
- (10) Halls, J. J. M.; Walsh, C. A.; Greenham, N. C.; Marseglia, E. A.; Friend, R. H.; Moratti, S. C.; Holmes, A. B. Efficient Photodiodes from Interpenetrating Polymer Networks. *Nature* **1995**, *376*, 498–500.
- (11) Cheng, Y.-J.; Yang, S.-H.; Hsu, C.-S. Synthesis of Conjugated Polymers for Organic Solar Cell Applications. *Chem. Rev.* **2009**, *109*, 5868–5923.
- (12) Roncali, J. Molecular Bulk Heterojunctions: An Emerging Approach to Organic Solar Cells. *Accounts Chem. Res.* **2009**, *42*, 1719–1730.
- (13) Li, Y.; Guo, Q.; Li, Z.; Pei, J.; Tian, W. Solution Processable D–A Small Molecules for Bulk-heterojunction Solar Cells. *Energ. Environ. Sci.* **2010**, *3*, 1427–1436.
- (14) Walker, B.; Kim, C.; Nguyen, T.-Q. Small Molecule Solution-Processed Bulk Heterojunction Solar Cells †. *Chem. Mater.* **2011**, *23*, 470–482.
- (15) Mishra, A.; Bäuerle, P. Small Molecule Organic Semiconductors on the Move: Promises for Future Solar Energy Technology. *Angew. Chem. Int. Ed.* **2012**, *51*, 2020–2067.

- 1
2
3
4 (16) Lin, Y.; Li, Y.; Zhan, X. Small Molecule Semiconductors for High-efficiency Organic
5 Photovoltaics. *Chem. Soc. Rev.* **2012**, *41*, 4245–4272.
6
7
8
9 (17) Kan, B.; Zhang, Q.; Li, M.; Wan, X.; Ni, W.; Long, G.; Wang, Y.; Yang, X.; Feng, H.;
10 Chen, Y. Solution-Processed Organic Solar Cells Based on Dialkylthiol-Substituted
11 Benzodithiophene Unit with Efficiency Near 10%. *J. Am. Chem. Soc.* **2014**, *136*, 15529–
12 15532.
13
14
15
16
17 (18) Po, R.; Roncali, J. Beyond Efficiency: Scalability of Molecular Donor Materials for
18 Organic Photovoltaics. *J. Mater. Chem. C* **2016**, *4*, 3677–3685.
19
20
21
22 (19) Bui, T.-T.; Goubard, F. Recent Advances in Small Molecular, Non-Polymeric Organic
23 Hole Transporting Materials for Solid-State DSSC. *EPJ Photovolt.* **2013**, *4*, 40402.
24
25
26
27 (20) Beaujuge, P. M.; Fréchet, J. M. J. Molecular Design and Ordering Effects in π -
28 Functional Materials for Transistor and Solar Cell Applications. *J. Am. Chem. Soc.*
29 **2011**, *133*, 20009–20029.
30
31
32
33
34 (21) Leliège, A.; Régent, C.-H. L.; Allain, M.; Blanchard, P.; Roncali, J. Structural Modu-
35 lation of Internal Charge Transfer in Small Molecular Donors for Organic Solar Cells.
36 *Chemical Communications* **2012**, *48*, 8907–8909.
37
38
39
40
41 (22) Inostroza, N.; Mendizabal, F.; Arratia-Pérez, R.; Orellana, C.; Linares-Flores, C. Im-
42 provement of Photovoltaic Performance by Substituent Effect of Donor and Acceptor
43 Structure of TPA-Based Dye-Sensitized Solar Cells. *J. Mol. Model.* **2016**, *22*, 1–7.
44
45
46
47
48 (23) Roncali, J.; Leriche, P.; Blanchard, P. Molecular Materials for Organic Photovoltaics:
49 Small is Beautiful. *Adv. Mater.* **2014**, *26*, 3821–3838.
50
51
52
53 (24) Demeter, D.; Mohamed, S.; Diac, A.; Grosu, I.; Roncali, J. Small Molecular Donors for
54 Organic Solar Cells Obtained by Simple and Clean Synthesis. *ChemSusChem* **2014**, *7*,
55 1046–1050.
56
57
58
59
60

- 1
2
3
4 (25) Zhang, X.; Grätzel, M.; Hua, J. Donor Design and Modification Strategies of Metal-
5 Free Sensitizers for Highly-Efficient n-type Dye-Sensitized Solar Cells. *Front. Optoelec.*
6 **2016**, *9*, 3–37.
7
8
9
10 (26) Mahmood, A. Triphenylamine Based Dyes for Dye Sensitized Solar Cells: A review.
11 *Sol. Energy* **2016**, *123*, 127–144.
12
13
14
15 (27) Quinton, C.; Alain-Rizzo, V.; Dumas-Verdes, C.; Clavier, G.; Vignau, L.; Audebert, P.
16 Triphenylamine/tetrazine Based π -Conjugated Systems as Molecular Donors for Or-
17 ganic Solar Cells. *New J. Chem.* **2015**, *39*, 9700–9713.
18
19
20
21
22 (28) Yen, Y.-S.; Chou, H.-H.; Chen, Y.-C.; Hsu, C.-Y.; Lin, J. T. Recent Developments
23 in Molecule-Based Organic Materials for Dye-Sensitized Solar Cells. *J. Mater. Chem.*
24 **2012**, *22*, 8734–8747.
25
26
27
28
29 (29) Liang, M.; Chen, J. Arylamine Organic Dyes for Dye-Sensitized Solar Cells. *Chemical*
30 *Society Reviews* **2013**, *42*, 3453–3488.
31
32
33
34 (30) Roquet, S.; Cravino, A.; Leriche, P.; Alévêque, O.; Frère, P.; Roncali, J.
35 Triphenylamine-Thienylenevinylene Hybrid Systems with Internal Charge Transfer as
36 Donor Materials for Heterojunction Solar Cells. *J. Am. Chem. Soc.* **2006**, *128*, 3459–
37 3466.
38
39
40
41
42
43 (31) Luponosov, Y. N.; Solodukhin, A. N.; Ponomarenko, S. A. Branched Triphenylamine-
44 Based Oligomers for Organic Electronics. *Polym. Sci. Ser. C* **2014**, *56*, 104–134.
45
46
47
48 (32) Jiang, Y.; Cabanetos, C.; Allain, M.; Liu, P.; Roncali, J. Manipulation of the Band Gap
49 and Efficiency of a Minimalist Push–Pull Molecular Donor for Organic Solar Cells. *J.*
50 *Mater. Chem. C* **2015**, *3*, 5145–5151.
51
52
53
54
55 (33) Leliège, A.; Grolleau, J.; Allain, M.; Blanchard, P.; Demeter, D.; Rousseau, T.; Ron-

- 1
2
3 cali, J. Small D- π -A Systems with o-Phenylene-Bridged Accepting Units as Active
4 Materials for Organic Photovoltaics. *Chem.-Eur. J.* **2013**, *19*, 9948–9960.
5
6
7
8
9 (34) Mohamed, S.; Demeter, D.; Laffitte, J.-A.; Blanchard, P.; Roncali, J. Structure-
10 properties Relationships in Triarylamine-Based Donor-Acceptor Molecules Containing
11 Naphtyl Groups as Donor Material for Organic Solar Cells. *Sci. Rep.* **2015**, *5*, 1–6.
12
13
14
15 (35) Chi, W.-J.; Li, Z.-S. The Theoretical Investigation on the 4-(4-phenyl-4- α -
16 naphthylbutadieny)-triphenylamine Derivatives as Hole Transporting Materials for
17 Perovskite-Type Solar Cells. *Phys. Chem. Chem. Phys.* **2015**, *17*, 5991–5998.
18
19
20
21
22 (36) Alberga, D.; Mangiatordi, G. F.; Labat, F.; Ciofini, I.; Nicolotti, O.; Lattanzi, G.;
23 Adamo, C. Theoretical Investigation of Hole Transporter Materials for Energy Devices.
24 *J. Phys. Chem. C* **2015**, *119*, 23890–23898.
25
26
27
28
29 (37) Yang, X.; Li, Q.; Shuai, Z. Theoretical Modelling of Carrier Transports in Molecular
30 Semiconductors: Molecular Design of Triphenylamine Dimer Systems. *Nanotechnology*
31 **2007**, *18*, 424029.
32
33
34
35
36 (38) Morvillo, P.; Bobeico, E. Tuning the LUMO Level of the Acceptor to Increase the
37 Open-Circuit Voltage of Polymer-Fullerene Solar Cells: A Quantum Chemical Study.
38 *Sol. Energy Mater. Sol. Cells* **2008**, *92*, 1192–1198.
39
40
41
42
43 (39) Alberga, D.; Perrier, A.; Ciofini, I.; Mangiatordi, G. F.; Lattanzi, G.; Adamo, C.
44 Morphological and Charge Transport Properties of Amorphous and Crystalline P3HT
45 and PBTTT: Insights From Theory. *Phys. Chem. Chem. Phys.* **2015**, *17*, 18742–18750.
46
47
48
49
50 (40) Zhang, L.; Shen, W.; He, R.; Liu, X.; Tang, X.; Yang, Y.; Li, M. Fine Structural Tuning
51 of Diketopyrrolopyrrole-Cored Donor Materials for Small Molecule-Fullerene Organic
52 Solar Cells: A Theoretical Study. *Org. Electron.* **2016**, *32*, 134–144.
53
54
55
56
57
58
59
60

- 1
2
3
4 (41) Zhang, L.; Shen, W.; He, R.; Tang, X.; Yang, Y.; Li, M. Density Functional Study
5 on The Effect of Aromatic Rings Flanked by Bithiophene of Novel Electron Donors in
6 Small-molecule Organic Solar Cells. *Mat. Chem. and Physics* **2016**, *175*, 13–21.
7
8
9
10 (42) Marcus, R. A. Electron Transfer Reactions in Chemistry. Theory and Experiment. *Rev.*
11 *Mod. Phys.* **1993**, *65*, 599–610.
12
13
14 (43) Rühle, V.; Lukyanov, A.; May, F.; Schrader, M.; Vehoff, T.; Kirkpatrick, J.;
15 Baumeier, B.; Andrienko, D. Microscopic Simulations of Charge Transport in Disor-
16 dered Organic Semiconductors. *J. Chem. Theory Comput.* **2011**, *7*, 3335–3345.
17
18
19 (44) Stehr, V.; Fink, R. F.; Engels, B.; Pflaum, J.; Deibel, C. Singlet Exciton Diffusion in
20 Organic Crystals Based on Marcus Transfer Rates. *J. Chem. Theory Comput.* **2014**,
21 *10*, 1242–1255.
22
23
24 (45) Kirkpatrick, J. An Approximate Method for Calculating Transfer Integrals Based on
25 the ZINDO Hamiltonian. *Int. J. Quantum Chem.* **2007**, *108*, 51–56.
26
27
28
29 (46) Baumeier, B.; Kirkpatrick, J.; Andrienko, D. Density-functional Based Determina-
30 tion of Intermolecular Charge Transfer Properties for Large-Scale Morphologies. *Phys.*
31 *Chem. Chem. Phys.* **2010**, *12*, 11103–11113.
32
33
34 (47) Poelking, C.; Andrienko, D. Effect of Polymorphism, Regioregularity and Paracrys-
35 tallinity on Charge Transport in Poly(3-hexylthiophene) [P3HT] Nanofibers. *Macro-*
36 *molecules* **2013**, *46*, 8941–8956.
37
38
39 (48) Poelking, C.; Cho, E.; Malafeev, A.; Ivanov, V.; Kremer, K.; Risko, C.; Brédas, J.-
40 L.; Andrienko, D. Characterization of Charge-Carrier Transport in Semicrystalline
41 Polymers: Electronic Couplings, Site Energies, and Charge-Carrier Dynamics in
42 Poly(bithiophene- alt -thienothiophene) [PBTTT]. *J. Phys. Chem. C* **2013**, *117*, 1633–
43
44
45
46
47
48
49
50
51
52
53
54
55
56
57
58
59
60

- 1
2
3
4 (49) Yavuz, I.; Martin, B. N.; Park, J.; Houk, K. N. Theoretical Study of the Molecular
5 Ordering, Paracrystallinity, And Charge Mobilities of Oligomers in Different Crystalline
6 Phases. *J. Am. Chem. Soc.* **2015**, *137*, 2856–2866.
7
8
9
10 (50) Materials Studio, Accelrys, San Diego, 2005.
11
12
13 (51) Perdew, J. P.; Burke, K.; Ernzerhof, M. Generalized Gradient Approximation Made
14 Simple. *Phys. Rev. Lett.* **1996**, *77*, 3865–3868.
15
16
17
18 (52) Mayo, S. L.; Olafson, B. D.; Goddard, W. A. DREIDING: a Generic Force Field for
19 Molecular Simulations. *J. Phys. Chem.* **1990**, *94*, 8897–8909.
20
21
22
23 (53) Sokolov, A. N.; Atahan-Evrenk, S.; Mondal, R.; Akkerman, H. B.; Sánchez-
24 Carrera, R. S.; Granados-Focil, S.; Schrier, J.; Mannsfeld, S. C.; Zoombelt, A. P.;
25 Bao, Z.; Aspuru-Guzik, A. From Computational Discovery to Experimental Character-
26 ization of a High Hole Mobility Organic Crystal. *Nat. Comm.* **2011**, *2*, 1–8.
27
28
29
30 (54) Zhang, B.; Kan, Y.-H.; Geng, Y.; Duan, Y.-A.; Li, H.-B.; Hua, J.; Su, Z.-M. An Efficient
31 Strategy for Improving Carrier Transport Performance – Introducing Fluorine Into Aryl
32 Substituted Tetracene. *Org. Electron.* **2013**, *14*, 1359–1369.
33
34
35
36 (55) Alberga, D.; Mangiatordi, G. F.; Torsi, L.; Lattanzi, G. Effects of Annealing and Resid-
37 ual Solvents on Amorphous P3HT and PBTTT Films. *J. Phys. Chem. C* **2014**, *118*,
38 8641–8655.
39
40
41
42 (56) Phillips, J. C.; Braun, R.; Wang, W.; Gumbart, J.; Tajkhorshid, E.; Villa, E.;
43 Chipot, C.; Skeel, R. D.; Kalé, L.; Schulten, K. Scalable Molecular Dynamics with
44 NAMD. *J. Comput. Chem.* **2005**, *26*, 1781–1802.
45
46
47
48 (57) Vanommeslaeghe, K.; Hatcher, E.; Acharya, C.; Kundu, S.; Zhong, S.; Shim, J.; Dar-
49 ian, E.; Guvench, O.; Lopes, P.; Vorobyov, I.; Mackerell, A. D. CHARMM General
50
51
52
53
54
55
56
57
58
59
60

- 1
2
3 Force Field: A Force Field for Drug-Like Molecules Compatible with the CHARMM
4 All-Atom Additive Biological Force Fields. *J. Comput. Chem.* **2009**, 671–690.
5
6
7
8
9 (58) Yu, W.; He, X.; Vanommeslaeghe, K.; MacKerell, A. D. Extension of the CHARMM
10 General Force Field to Sulfonyl-Containing Compounds and its Utility in Biomolecular
11 Simulations. *J. Comput. Chem.* **2012**, *33*, 2451–2468.
12
13
14
15 (59) Bayly, C. I.; Cieplak, P.; Cornell, W.; Kollman, P. A. A Well-Behaved Electrostatic
16 Potential Based Method Using Charge Restraints for Deriving Atomic Charges: the
17 RESP Model. *J. Phys. Chem.* **1993**, *97*, 10269–10280.
18
19
20
21
22 (60) Coropceanu, V.; Cornil, J.; da Silva Filho, D. A.; Olivier, Y.; Silbey, R.; Brédas, J.-L.
23 Charge Transport in Organic Semiconductors. *Chemical Reviews* **2007**, *107*, 926–952.
24
25
26
27 (61) Besler, B. H.; Merz, K. M.; Kollman, P. A. Atomic Charges Derived from Semiempirical
28 Methods. *J. Comput. Chem.* **1990**, *11*, 431–439.
29
30
31
32 (62) Malagoli, M.; Coropceanu, V.; da Silva Filho, D. A.; Brédas, J. L. A Multimode Anal-
33 ysis of the Gas-Phase Photoelectron Spectra in Oligoacenes. *The Journal of Chemical*
34 *Physics* **2004**, *120*, 7490.
35
36
37
38
39 (63) Rosso, K. M.; Dupuis, M. Electron Transfer in Environmental Systems: a Frontier for
40 Theoretical Chemistry. *Theor. Chem. Acc.* **2005**, *116*, 124–136.
41
42
43
44 (64) Sánchez-Carrera, R. S.; Coropceanu, V.; da Silva Filho, D. A.; Friedlein, R.; Osikow-
45 icz, W.; Murdey, R.; Suess, C.; Salaneck, W. R.; Brédas, J.-L. Vibronic Coupling in
46 the Ground and Excited States of Oligoacene Cations. *J. of Phys. Chem. B* **2006**, *110*,
47 18904–18911.
48
49
50
51
52
53 (65) Stehr, V.; Engels, B.; Deibel, C.; Fink, R. F. Anisotropy of Singlet Exciton Diffusion
54 in Organic Semiconductor Crystals From Ab Initio Approaches. *J. Chem. Phys.* **2014**,
55 *140*, 024503–1–024503–12.
56
57
58
59
60

- 1
2
3
4 (66) Fink, R. F.; Pfister, J.; Zhao, H. M.; Engels, B. Assessment of Quantum Chemical
5 Methods and Basis Sets for Excitation Energy Transfer. *Chem. Phys.* **2008**, *346*, 275–
6 285.
7
8
9
10 (67) Davydov, A. S. The Theory of Molecular Excitons. *Sov. Phys. Usp.* **1964**, *7*, 145–178.
11
12
13 (68) Tomasi, J.; Mennucci, B.; Cammi, R. Quantum Mechanical Continuum Solvation Mod-
14 els. *Chem. Rev.* **2005**, *105*, 2999–3094.
15
16
17
18 (69) Song, Y.; Lv, S.; Liu, X.; Li, X.; Wang, S.; Wei, H.; Li, D.; Xiao, Y.; Meng, Q. Energy
19 Level Tuning of TPB-Based Hole-Transporting Materials for Highly Efficient Perovskite
20 Solar Cells. *Chem. Commun.* **2014**, *50*, 15239–15242.
21
22
23
24
25 (70) Scholes, G. D.; Rumbles, G. Excitons in Nanoscale Systems. *Nat. Mater.* **2006**, *5*,
26 683–696.
27
28
29
30 (71) Alberga, D.; Mangiatordi, G. F.; Motta, A.; Nicolotti, O.; Lattanzi, G. Effects of Dif-
31 ferent Self-Assembled Monolayers on Thin-Film Morphology: A Combined DFT/MD
32 Simulation Protocol. *Langmuir* **2015**, *31*, 10693–10701.
33
34
35
36
37
38
39
40
41
42
43
44
45
46
47
48
49
50
51
52
53
54
55
56
57
58
59
60

Graphical TOC Entry

